Sunyaev-Zel'dovich profiles and scaling relations: modelling effects and observational biases

A. Bonaldi[1,2], G. Tormen[2], K. Dolag[3] and L. Moscardini[4,5]

[1] *INAF-Osservatorio Astronomico di Padova, vicolo dell'Osservatorio 5, I-35122 Padova, Italy (anna.bonaldi@oapd.inaf.it)*
[2] *Dipartimento di Astronomia, Università di Padova, vicolo dell'Osservatorio 2, I-35122 Padova, Italy (giuseppe.tormen@unipd.it)*
[3] *Max-Planck Institut fuer Astrophysik, Karl-Schwarzschild Strasse 1, D-85748 Garching, Germany (kdolag@mpa-garching.mpg.de)*
[4] *Dipartimento di Astronomia, Università di Bologna, via Ranzani 1, I-40127 Bologna, Italy (lauro.moscardini@unibo.it)*
[5] *INFN, Sezione di Bologna, viale Berti Pichat 6/2, I-40127 Bologna, Italy*

ABSTRACT

We use high-resolution hydrodynamic re-simulations to investigate the properties of the thermal Sunyaev-Zel'dovich (SZ) effect from galaxy clusters. We compare results obtained using different physical models for the intracluster medium (ICM), and show how they modify the SZ emission in terms of cluster profiles and scaling relations. We also produce realistic mock observations to verify whether the results from hydrodynamic simulations can be confirmed. We find that SZ profiles depend marginally on the modelled physical processes, while they exhibit a strong dependence on cluster mass. The central and total SZ emission strongly correlate with the cluster X-ray luminosity and temperature. The logarithmic slopes of these scaling relations differ from the self-similar predictions by less than 0.2; the normalization of the relations is lower for simulations including radiative cooling. The observational test suggests that SZ cluster profiles are unlikely to be able to probe the ICM physics. The total SZ decrement appears to be an observable much more robust than the central intensity, and we suggest using the former to investigate scaling relations.

Key words: cosmic microwave background – galaxies: clusters: general – hydrodynamics – methods: numerical

1 INTRODUCTION

Galaxy clusters are ideal probes for studies of large scale structures. They have typical masses of order $10^{14} - 10^{15} M_\odot$; within a radius of a few Mpc they contain hundreds of galaxies orbiting in a gravitational potential well due primarily to dark matter (DM). They are also filled with ICM: hot ionized gas, typically at a temperature of 1-15 keV, that can be observed via its bremsstrahlung emission in the soft X-ray band, and via the Sunyaev-Zel'dovich (SZ) effect in the millimetric band.

Several observational evidences demonstrate that the picture of an ICM in hydrostatic equilibrium in the DM potential well of the cluster is an over-simplification: above all, scaling relations between various cluster properties, like mass, temperature and X-ray luminosity, differ from the self-similar predictions (see, e.g., the recent reviews by Rosati et al. 2002; Voit 2005; Borgani 2006, and the references therein). In order to explain the ICM properties, many models have been developed so far, which consider the effect of radiative cooling and of non-gravitational heating (mainly feedback from supernovae and AGNs). As the complexity in the physical description of the ICM increased, hydrodynamic simulations have also improved to include such processes, and have become in-

valuable tools to compare theoretical predictions with current data and to forecast the performance of future experiments.

On the observational side, important improvements are expected for the detection of the SZ effect in clusters thanks to an upcoming new generation of suitable instruments, like AMI[1], SPT[2], ACT[3], SZA[4], AMiBA[5], APEX[6], and PLANCK[7]. In order to correctly extract and utilize the information contained in these data it will be mandatory to keep under control both the dependence of the SZ signal on the ICM physics, and the possible biases induced on the intrinsic signal by the details of the observational process.

In the present work we investigate how different choices for the physical modelling of the ICM affect the SZ radial profiles and the scaling relations between the SZ flux and other intrinsic properties of clusters. To this end, we use a set of high-resolution hydrodynamical simulations, where clusters were re-simulated including

[1] *http://www.mrao.cam.ac.uk/telescopes/ami/*
[2] *http://spt.uchicago.edu/*
[3] *http://www.hep.upenn.edu/act/*
[4] *http://astro.uchicago.edu/sza/*
[5] *http://amiba.asiaa.sinica.edu.tw/*
[6] *http://bolo.berkeley.edu/apexsz/*
[7] *http://www.rssd.esa.int/Planck/*

different physical processes, from radiative cooling, to star formation, energy feedback from supernovae, and thermal conduction.

After this analysis, we adopt the instrumental characteristics of the AMI interferometer and simulate the observational process for a few clusters in our sample: this enable us to discuss possible biases introduced in our results by a realistic observation process.

The present paper is organized as follows. After briefly introducing in Sect. 2 the SZ effect and the main related quantities, in Sect. 3 we describe the general characteristics of the hydrodynamic simulations used in our study. In Sect. 4 we obtain fitting formulas for the cluster SZ profiles, while in Sect. 5 we discuss the effects of various physical processes on the scaling relations between some global properties commonly used to describe galaxy clusters. In Sect. 6 we perform simulated observations assuming the characteristics of the AMI instrument, and discuss the robustness of our results. Finally in Sect. 7 we draw our conclusions.

2   THE SUNYAEV-ZEL'DOVICH EFFECT

The thermal SZ effect (Sunyaev & Zeldovich 1972) is a distorsion in the cosmic microwave background (CMB) spectrum due to inverse Compton scattering of CMB photons by hot ionized gas particles (for recent reviews see, e.g., Birkinshaw 1999; Carlstrom et al. 2002; Rephaeli et al. 2005). Its intensity is given by the Comptonization parameter y, defined as:

$$y \equiv \frac{k_B \sigma_T}{m_e c^2} \int n_e T_e dl \; , \tag{1}$$

where k_B is the Boltzmann constant, σ_T is the Thomson cross section, c is the speed of light, and n_e, T_e and m_e are the electronic number density, temperature and rest mass, respectively. As evident from Eq.(1), the y-parameter is directly proportional to the cluster pressure P integrated along the line of sight. The change in the CMB intensity at the frequency ν corresponding to a certain value of the Comptonization parameter is:

$$\Delta I_{\rm CMB} = \frac{2(k_B T)^3}{(hc)^2} g(x) \, y \; , \tag{2}$$

where h is the Planck constant. The frequency dependence is given by the spectral shape $g(x)$:

$$g(x) = \frac{x^4 e^x}{(e^x - 1)^2} \left(x \frac{e^x + 1}{e^x - 1} - 4 \right) \; , \tag{3}$$

where $x \equiv h\nu/k_B T_{\rm CMB}$.

In galaxy clusters the Comptonization parameter y typically reaches values of order 10^{-6} on arc-minute scales, corresponding to fluctuations in the CMB temperature of few μK. As a consequence, observing galaxy clusters through the SZ effect requires extremely good sensitivity, in order to obtain sufficiently high signal-to-noise ratios. The required sensitivity and sky coverage will be achieved in the near future, thanks to new dedicated instruments. Nevertheless, the resolution of these instruments will be not enough to detect the wealth of details which can be seen in numerical hydrodynamical simulations: substructures, shocks, etc. For this reason, in order to be meaningful and helpful, all analyses of the SZ effect based on simulations must deal with the actual instrumental capabilities: this is one of the main goals of this paper, as discussed below.

Table 1. Different physical processes included in our re-simulations

simulation name	involved physical processes
ovisc	non-radiative gas-dynamics with standard viscosity
lvisc	like *ovisc*, but with low viscosity
csf	cooling, star formation and feedback
csfc	like *csf* plus thermal conduction

3   PROPERTIES OF THE SIMULATED CLUSTERS

The hydrodynamic simulations used in the present work were carried out using GADGET-2 (Springel 2005), a new version of the parallel Tree+SPH (Smoothed Particle Hydrodynamics) code GADGET (Springel et al. 2001). GADGET-2 includes an entropy-conserving formulation of SPH (Springel & Hernquist 2002), radiative cooling, heating by an UV background, and a treatment of star formation and feedback from galactic winds powered by supernova explosions. The latter is based on a subresolution model for the multi-phase structure of the interstellar medium, as described in Springel & Hernquist (2003). The SPH implementation of thermal conduction in GADGET-2, which is both stable and manifestly conserves thermal energy - even when individual and adaptive time-steps are used - was described in Jubelgas et al. (2004). This implementation assumes an isotropic effective conductivity parameterized as a fixed fraction of the Spitzer rate. It also accounts for saturation, which can become relevant for low-density gas.

3.1   The sample of re-simulated clusters

The set of simulated galaxy clusters used in the following analysis includes 11 objects, which we divide in two samples: seven low-mass clusters, with virial mass $M_{\rm vir} \simeq 10^{14} h^{-1} M_\odot$ (LM sample), and four high-mass systems with $M_{\rm vir} = (1.3 - 2.3) \times 10^{15} h^{-1} M_\odot$ (HM sample). The cluster regions were extracted from a (DM-only) cosmological simulation (see Yoshida et al. 2001) with box-size $479 \, h^{-1} \, {\rm Mpc}$ of a flat ΛCDM model with matter density parameter $\Omega_{\rm 0m} = 0.3$, cosmological constant density parameter $\Omega_\Lambda = 0.7$, dimensionless Hubble parameter $h = 0.7$, power spectrum normalization $\sigma_8 = 0.9$ and baryon density parameter $\Omega_{\rm b} = 0.04$. Using the "Zoomed Initial Conditions" (ZIC) technique (Tormen et al. 1997), these regions were re-simulated at higher mass and force resolution by populating their Lagrangian volume in the initial conditions with a larger number of particles, while appropriately adding high-frequency modes. At the same time, the large-scale tidal field of the cosmological environment is correctly described by using low-resolution particles. The unperturbed particle distribution (before displacements) is of glass-type (White 1996). Gas was added only in the high-resolution region by splitting each original particle into a gas and a DM one. Thereby, the gas and the DM particles were displaced by half the original mean interparticle distance, so that the centre-of-mass and the momentum were conserved. Each gas particle has mass $m_{\rm gas} = 1.7 \times 10^8 \, h^{-1} \, M_\odot$, while the mass of the DM particles is $m_{\rm DM} = 1.13 \times 10^9 \, h^{-1} \, M_\odot$; thus, the total number of particles inside our simulated clusters is between 2×10^5 and 4×10^6, depending on their final mass. For all simulations, the gravitational softening length was kept fixed at $\epsilon = 30 \, h^{-1} \, {\rm kpc}$ comoving (Plummer-equivalent) for $z > 5$, and was switched to a physical softening length of $\epsilon = 5 \, h^{-1} \, {\rm kpc}$ at $z = 5$.

Each object of the cluster set was re-simulated four times, in-

Table 2. The sample of simulated clusters. For each object we report name, virial mass $M_{\rm vir}$, virial radius $R_{\rm vir}$, mass-weighted temperature T, X-ray luminosity L_X in the [0.1-10 keV] band, and central value y_0 of the Comptonization parameter. Clusters are divided in two samples depending on their mass: low-mass (LM) and high-mass (HM).

LM sample	$M_{\rm vir}$ [$M_\odot/h$]	$R_{\rm vir}$ [kpc/h]	T [keV]	L_X [erg/s]	y_0
g676	1.1×10^{14}	983	1.1	3.2×10^{44}	3.6×10^{-5}
g3344	1.1×10^{14}	1002	1.4	2.2×10^{44}	2.9×10^{-5}
g6212	1.1×10^{14}	1000	1.3	3.0×10^{44}	4.4×10^{-5}
g1542	1.1×10^{14}	982	1.3	3.0×10^{44}	4.2×10^{-5}
g1b	4.5×10^{14}	1585	2.6	4.2×10^{44}	5.0×10^{-5}
g1c	1.9×10^{14}	1181	1.4	3.0×10^{44}	4.3×10^{-5}
g1d	1.5×10^{14}	1098	1.2	1.0×10^{44}	1.4×10^{-5}
HM sample	$M_{\rm vir}$ [$M_\odot/h$]	$R_{\rm vir}$ [kpc/h]	T [keV]	L_X [erg/s]	y_0
g8a	2.4×10^{15}	2758	10.6	8.1×10^{45}	7.4×10^{-4}
g1a	1.5×10^{15}	2358	7.0	4.8×10^{45}	4.3×10^{-4}
g51a	1.3×10^{15}	2276	6.2	3.2×10^{45}	3.5×10^{-4}
g72a	1.4×10^{15}	2299	5.8	1.8×10^{45}	1.9×10^{-4}

cluding a different set of physical processes for the gas component (see the list in Table 1). Both simulations referred as *ovisc* and *lvisc* follow non-radiative gas-dynamics: for *ovisc* a standard viscosity scheme is adopted, while *lvisc* runs were carried out using a modified artificial viscosity scheme suggested by Morris & Monaghan (1997), where each particle evolves in time its individual viscosity parameter. Whereas in this scheme shocks are as well captured as in the standard scheme, regions with no shocks do not suffer for residual non-vanishing artificial viscosity. Therefore, turbulence driven by fluid instabilities can be much better resolved by the new scheme and, as a result of this, galaxy clusters can build up a sufficient level of turbulence-powered instabilities along the surfaces of the large-scale velocity structure present in cosmic structure formation (Dolag et al. 2005). In simulations which include star formation and feedback (*csf* and *csfc*), the supernovae efficiency in powering galactic winds was set to 50 per cent, which corresponds to a wind speed of about 340 km s^{-1}. For the *csfc* simulations, which also include the effect of thermal conduction, we assume a fixed fraction 1/3 of the Spitzer rate. A more detailed description of the properties of simulated galaxy clusters including thermal conduction can be found in Dolag et al. (2004).

Table 2 summarizes the main properties of the 11 clusters, obtained using the *ovisc* simulation. In particular, for each object we list its virial mass $M_{\rm vir}$, virial radius $R_{\rm vir}$, mass-weighted temperature T, X-ray luminosity L_X in the [0.1-10 keV] band, and central value y_0 of the Comptonization parameter. Notice that both T and L_X are computed inside $R_{\rm vir}$, which was defined using the overdensity threshold dictated by the spherical top-hat model (see, e.g., Eke et al. 1996). The same properties in simulations with a different ICM modelling show discrepancies at most of few per cent for virial masses and mass-weighted temperatures. Conversely, typical X-ray luminosities, when compared to the *ovisc* runs, are reduced on average by a factor of 2 in the *lvisc* simulations and by a factor of 5 in both the *csf* and *cfsc* runs.

4   FITTING RADIAL PROFILES

In this section we discuss the procedure adopted to find fitting relations for the radial profiles of the SZ maps of our clusters. To produce two-dimensional (2D) SZ maps we followed a standard procedure which employs the SPH kernel to distribute the desired

quantities (in this case the Comptonization parameter y), on a grid. Details on the method may be found in Dolag et al. (2006) and Roncarelli et al. (2006). In particular, we considered the simulation outputs at $z = 0$, and for each cluster we obtained three SZ maps, corresponding to projections along the cartesian axes. The SZ maps, 4 Mpc on a side, were integrated over 8 Mpc along the line of sight: we checked that such integration is enough to enclose most of the cluster signal, so that no artificial cutoff is introduced.

Examples of SZ maps are shown on the right column of Fig.1, where we present two systems, *g1a* (upper panels) and *g1c* (bottom panels), representative of the HM and LM samples, respectively. In both cases we show the output of the non-radiative simulation *ovisc*. For completeness we also display the corresponding 2D maps for the gas density (left column) and for the mass-weighted temperature (central column).

The radial profiles obtained from the SZ maps are strongly dependent on the cluster mass: for this reason we decided to obtain fitting profiles for the LM and HM samples separately. In order to obtain best-fitting relations for the profiles of the Comptonization parameter y, we started from three-dimensional (3D) data, and built a model for the SZ emission directly linked to the 3D cluster shape. In particular, we obtained the 3D pressure profile for each cluster of our sample and fit it using a simple analytical formula, which we then integrated along the line of sight. As we are going to show, the resulting expression, evaluated at the correct integration limits, provides a good fit for the SZ radial profiles.

The 3D pressure profiles of each cluster were obtained by calculating the mean value of ϱT for particles in spherical shells of equal logarithmic width out to $4R_{\rm vir}$. In order to extract a mean profile for each mass bin, and for each set-up of the physical processes, we need to appropriately normalize each profile, obtaining dimensionless quantities. Assuming a self-similar model for the density profiles, differences in pressure are due to differences in temperature only. We found that the resulting pressure profiles for our simulated clusters, however, do not properly superimpose when normalized by their temperature, indicating that also density profiles show non-negligible deviations from a self-similar behaviour. For this reason we preferred to use an empirical normalization, adopting the value of the pressure integrated up to a given fixed radius. We chose R_{500}, the radius at which the mean overdensity of the cluster is 500 times the critical density of the universe (roughly corresponding to 60 per cent of $R_{\rm vir}$). The normalization factor ob-
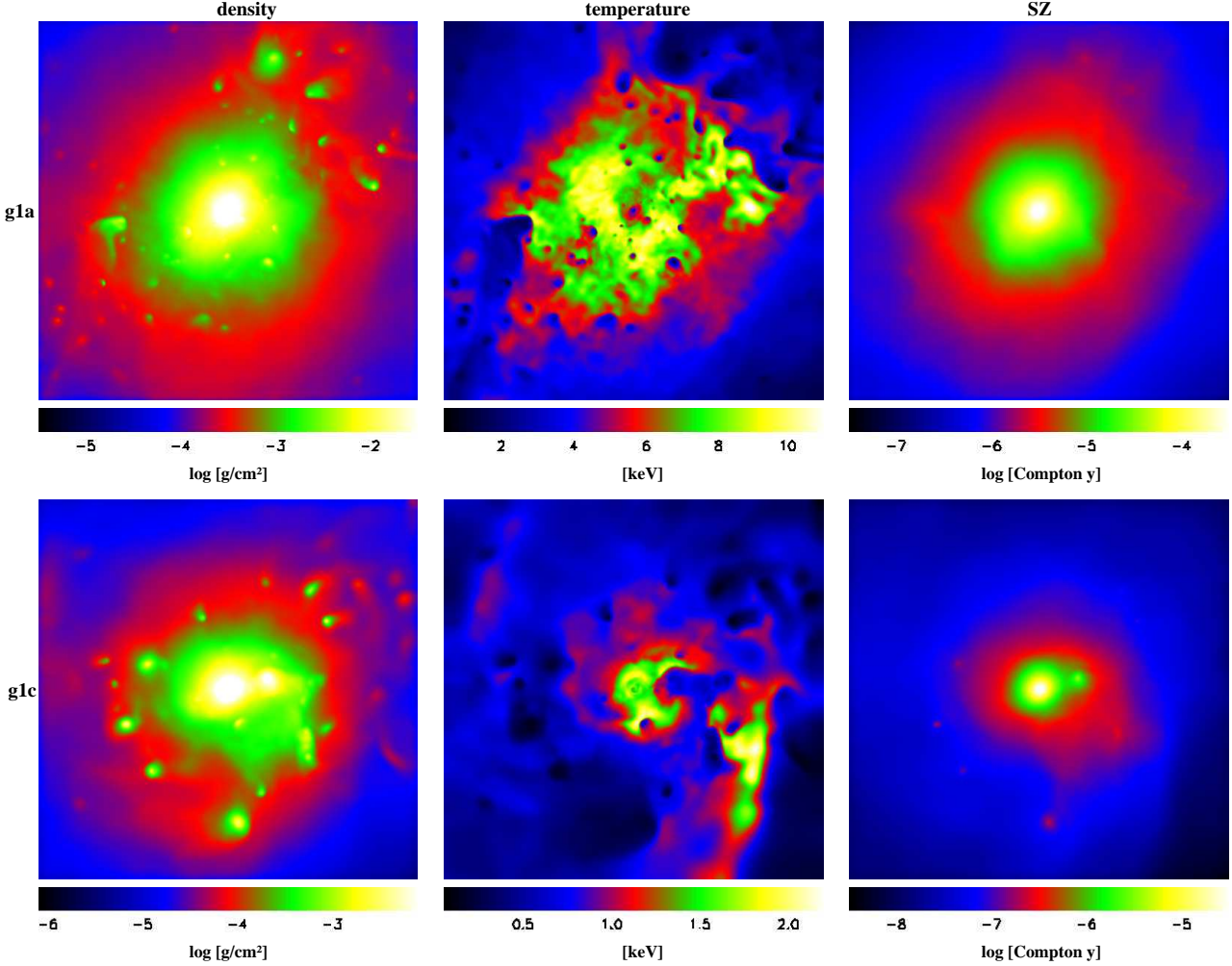
Figure 1. Projected maps of gas density (left column), mass-weighted temperature (central column) and Comptonization parameter y (right column) for two galaxy clusters: *g1a* (top panels) and *g1c* (bottom panels), both taken at $z = 0$ and considering the non-radiative simulation *ovisc*. The displayed region is a square with side 4 Mpc. The colour scale is shown at the bottom of each panel.

tained in this way for each cluster was also used to obtain the mean SZ profiles.

After obtaining a mean 3D profile for each cluster subsample, we looked for a fitting relation that is also integrable along the line of sight. We chose the following expression for the 3D fit in spherical coordinates (R, θ, ϕ):

$$F(R) = I_{3D}(R + r_p)^b + K \,, \tag{4}$$

where $R = \sqrt{x^2 + y^2 + z^2}$ is the 3D clustercentric distance (in units of the virial radius R_{vir}) and I_{3D} is the intensity normalization factor. The free parameters used for the fit are three: r_p (also given in units of R_{vir}), b and K.

In order to obtain the SZ map fitting relation we rewrite Eq.(4) in cylindrical coordinates (r, θ, z) and integrate along z, obtaining:

$$
\begin{aligned}
f(r) &= I_{2D} \int_{l_1}^{l_2} F(r, z)dz = \\
&= I_{2D} \left[\left(r_p + \sqrt{r^2 + z^2} \right)^{(b-1)} + Kz \right]_{z=l_1}^{z=l2} , \tag{5}
\end{aligned}
$$

where $r = \sqrt{x^2 + y^2}$ is the 2D clustercentric distance (again in units of the virial radius R_{vir}) and l_1, l_2 are the integration lim-

its adopted. From a theoretical point of view, integration along the line of sight should be performed from the centre to infinity. For practical reasons, however, the outer limit can be safely set to a radius above which the intensity does not significantly contribute to the result: in our case we choose $l_2 = 2 \times R_{\mathrm{vir}}$. As for the inner limit, the 3D profile in the simulations can be robustly computed only down to radii enclosing at least of order of 100 particles, so our fitting profile for $R \rightarrow 0$ is actually an extrapolation. In particular, the contribution from the cluster centre to the integral along the z-axis leads to errors in the SZ profile. However, if we give up integrating down to $z \rightarrow 0$, we can minimize the contribution from $R \rightarrow 0$ and get a correct integrated profile. For this reason we used $l_1 = 0.015R_{\mathrm{vir}}$ and we accounted for the flux underestimation in the factor I_{2D}.

As an example, in Fig. 2 we show radial profiles for the pressure P and for the Comptonization parameter y (left and right panels, respectively). Results are displayed for the physical model *ovisc* and for both cluster samples: LM (upper panels) and HM (lower panels). Solid lines indicate the mean of the logarithmic profiles, with corresponding 1σ error bars, while dashed lines show the fitting relations obtained using Eqs.(4) and (5). We notice that the
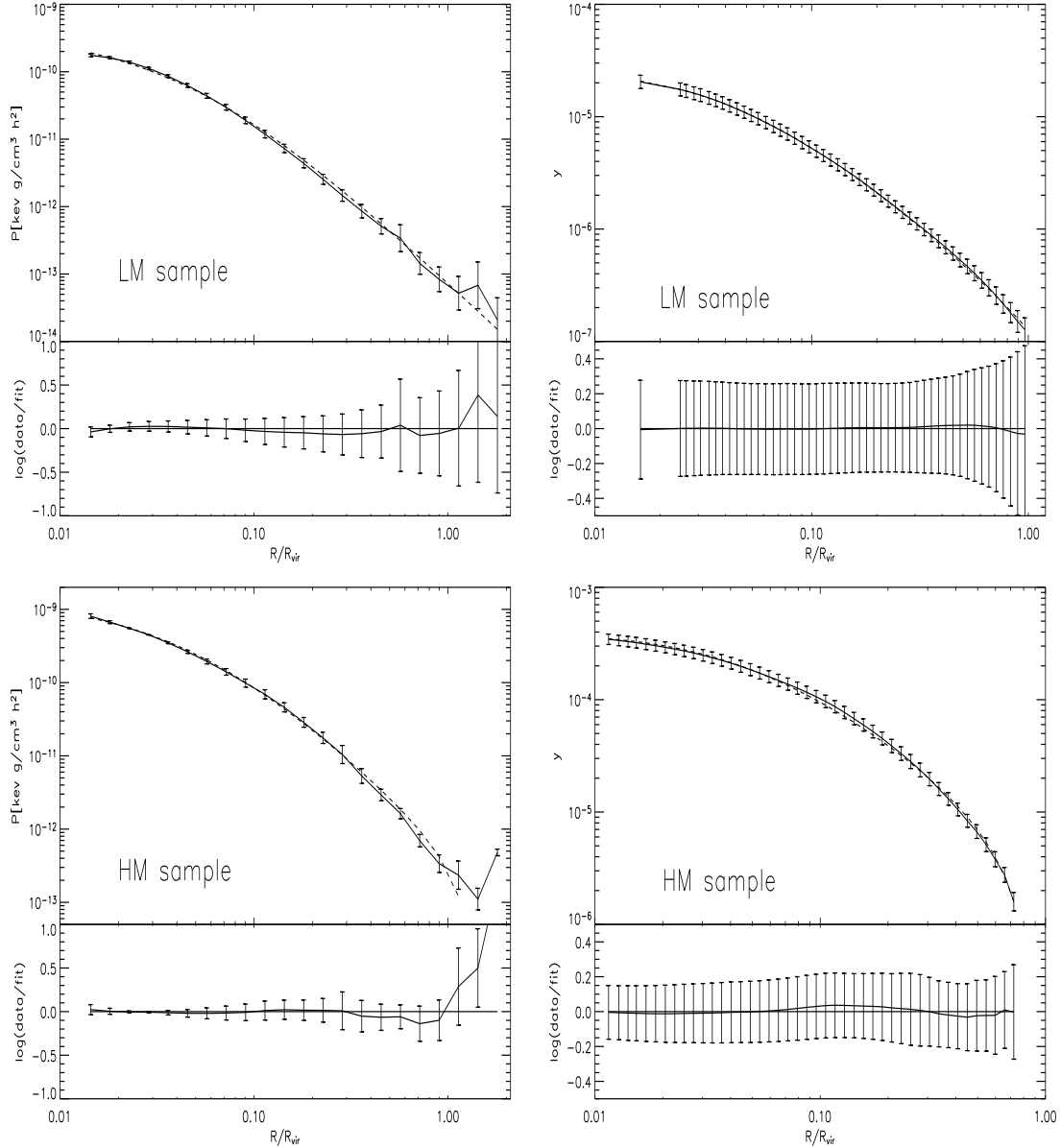
Figure 2. The radial profiles for 3D pressure P (left panels) and for the Comptonization parameter y (right panels) as obtained from the *ovisc* simulations. Upper and lower panels refer to the LM and HM samples, respectively. Solid and dashed lines are the mean of the logarithmic profiles and our fitting relations, respectively. Error bars show error on the mean. The smaller box below each panel shows the mean of the logarithmic residuals with the corresponding root mean square (rms) value.

3D fit is not always within the error bars: this is mainly due to the noisy tail of the pressure profile outside R_{vir}. Our interpretation is confirmed by looking at the logarithmic residuals shown in the smaller box below each panel: here we plot their mean and rms values. At any rate, we will see that SZ profiles are more regular, as a result of the integration process, and the integrated relation will be an extremely good fit.

Extending our analysis to the simulations which include different physical processes, we computed the fitting parameters which let us derive the 3D fitting profiles according to Eq.(4), and the 2D ones according to Eq.(5). The results are summarized in Table 3.

The resulting SZ profiles for all physics are plotted in Fig.3,

for both mass bins. We find that differences due to cluster physics are mainly visible in the low-mass clusters, and affect in particular the inner region of the profiles: therefore such differences are unlikely to be probed through observations (see the discussion below). We also note that, for both mass bins, the models *csf* and *csfc* have the same r_p, b, and K, and only slightly differ in intensity I_{2D}. This is due to the fact that thermal conduction acts mainly locally, so it does not significantly affect quantities averaged on sufficiently large scales, like the radial SZ profile.
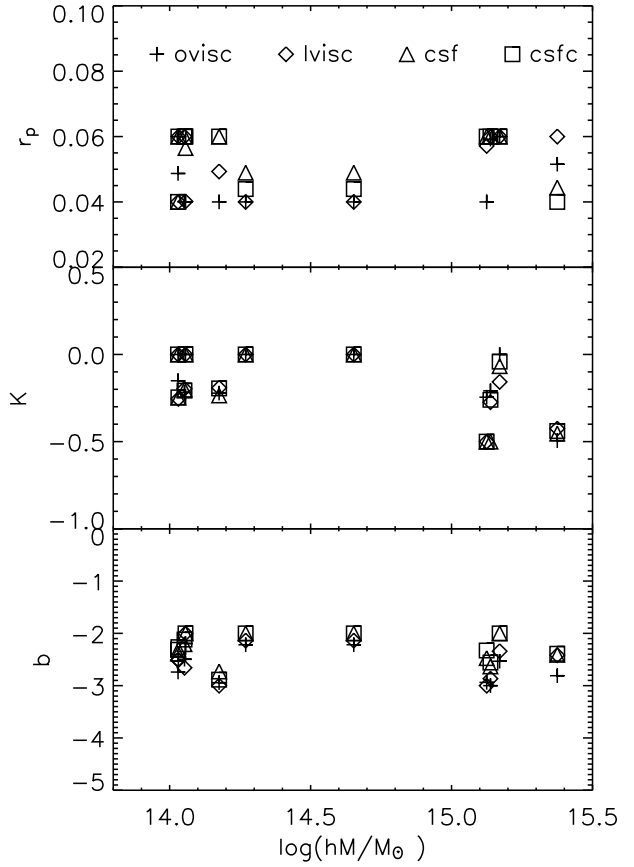
As we stated above, there is a significant difference between the mean profiles obtained for high- and low-mass clusters, as clearly shown in Fig. 3. We note that there is also a selection effect which may be responsible for this effect: the HM clusters of our

Table 3. Fitting parameters for 3D and 2D profiles (Eqs.(4) and (5), respectively).

| Cluster sample	Physics	$I_{3D}[\text{erg/cm}^3]$	I_{2D}	r_p	b	K
LM sample	*ovisc*	7.48×10^{-14}	1.83×10^{-7}	0.045	-2.75	0.0
	lvisc	8.93×10^{-14}	1.88×10^{-7}	0.075	-2.9	0.0
	csf	1.00×10^{-13}	2.36×10^{-7}	0.06	-2.55	0.0
	csfc	8.10×10^{-14}	1.99×10^{-7}	0.06	-2.55	0.0
HM sample	*ovisc*	6.37×10^{-13}	3.94×10^{-6}	0.05	-2.6	-0.45
	lvisc	6.56×10^{-13}	5.26×10^{-6}	0.08	-2.6	-0.45
	csf	6.56×10^{-13}	3.52×10^{-6}	0.09	-2.8	-0.45
	csfc	6.43×10^{-13}	3.74×10^{-6}	0.09	-2.8	-0.45
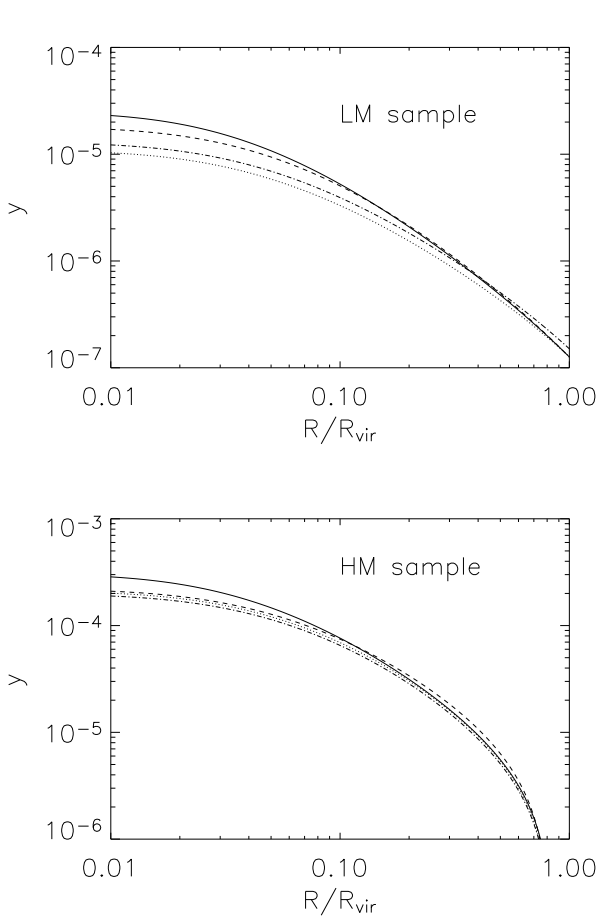
Figure 3. Comparison between the mean logarithmic SZ profiles obtained from cluster simulations including different ICM modelling: *ovisc* (solid line), *lvisc* (dashed line), *csf* (dashed-dotted), *csfc* (dotted line). Upper and lower panels refer to LM and HM samples, respectively.

Figure 4. Mass dependence of the fitting parameters r_p (upper panel), K (central panel) and b (lower panel). Different symbols refer to simulations with different physical processes included, as indicated in the upper panel.

re-simulations, infact, have been chosen to be relaxed and isolated, while the LM clusters have more varied dynamical configurations. As also pointed out by Rasia et al. (2004), the density profiles in the external regions are on average steeper for isolated systems than for objects having more general environmental situations. This property, then, reflects in our SZ profiles. Specifically, profiles of both subsamples have a logarithmic slope going to 0 as $R/R_{\text{vir}} \to 0$. The slope of the LM sample steepens at $R/R_{\text{vir}} = 0.04 - 0.07$ and then remains nearly constant up to R_{vir}. Conversely, the slope

of the profiles in the HM sample presents a first steepening at $R/R_{\text{vir}} = 0.05 - 0.09$ and a second one at $R/R_{\text{vir}} \sim 0.6$. To reproduce this feature we had to add a negative constant (K) to the fitting relations.

This result suggests that the fitting parameters r_p, b and K might depend on the cluster mass. To investigate whether this is true, we fitted relations like Eq.(5) to all individual SZ profiles, and plotted in Fig. 4 the resulting parameters vs. cluster mass. Since the mean profiles depend only mildly on the cluster physics, we prefer to show the data coming from the different re-simulations together, thus increasing our statistics. Plotting the parameters r_p, K and b against the (logarithm of the) mass we do not find any
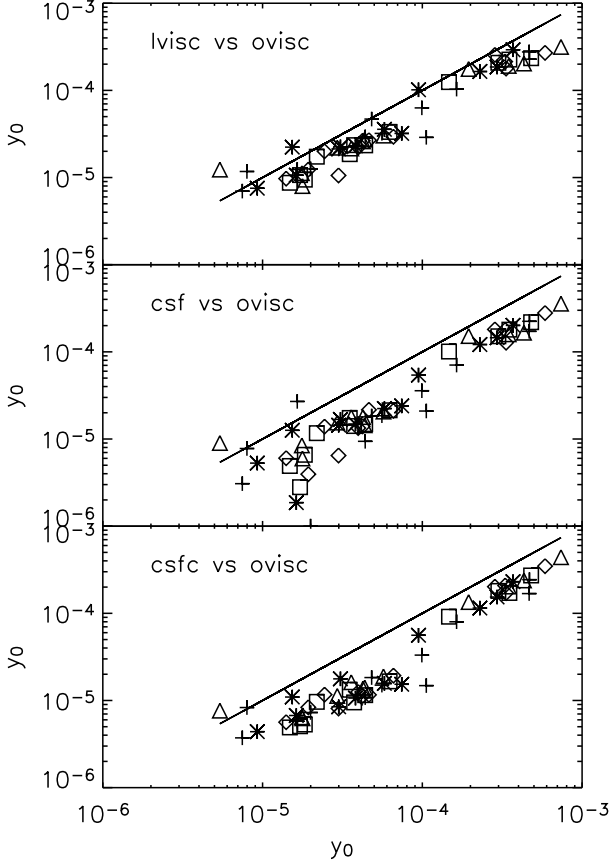
Figure 5. Comparison of the values y_0 obtained for a given cluster in the *ovisc* simulation (horizontal axis) with the corresponding values obtained in the other simulations (vertical axes): *lvisc* (top panel), *csf* (central panel) and *csfc* (bottom panel). Different symbols refer to clusters observed at different redshifts: $z = 0$ (crosses), $z = 0.2$ (stars), $z = 0.4$ (squares), $z = 0.7$ (diamonds) and $z = 1$ (triangles). The solid line corresponds to the bisecting line.

Figure 6. As Fig.5, but for ΔS.

statistically significant trend. However, we notice that, as suggested by the comparison of the mean profiles, higher masses correspond on average to higher values for the scale radius r_p and to steeper profiles at $R/R_{\rm vir} \rightarrow 1$, as shown by the higher (absolute) value assumed by K.
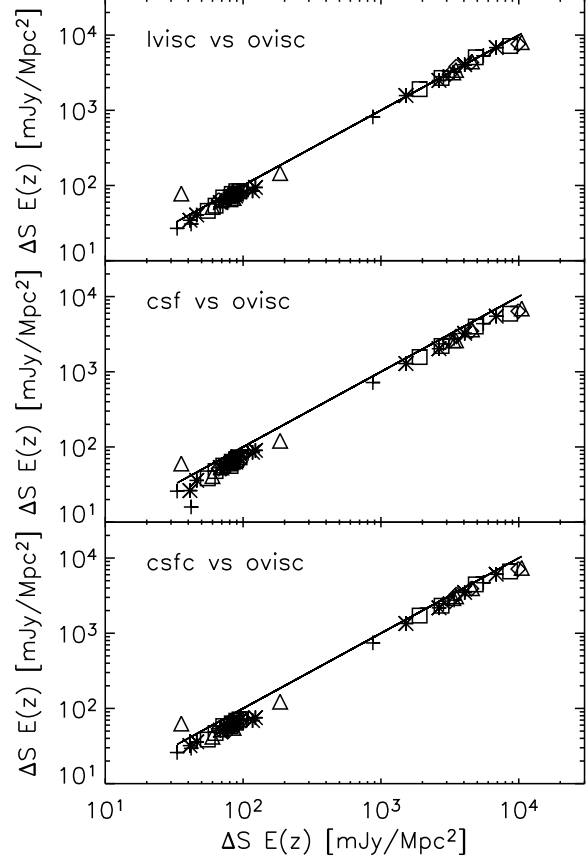
5 SZ SCALING RELATIONS

If gravity is the only physical process in action during their formation, galaxy clusters can be modelled using the so-called self-similar model (Kaiser 1986; Navarro et al. 1995), which predicts simple scaling relations between the main cluster properties (mass, temperature, etc.). In particular, in terms of SZ and X-ray observables, the self-similar model suggests the following relations:

$$y_0 \quad \propto L_X^{3/4} E^{1/4}(z) \,, \tag{6}$$

$$y_0 \quad \propto T^{3/2} E(z) \,, \tag{7}$$

$$\Delta S \quad \propto T^{5/2} E^{-1}(z) \,. \tag{8}$$

In the previous equations y_0 is the central value for the Comptonization parameter y, ΔS is the SZ flux integrated out to a given radius, T is the ICM temperature, L_X is the X-ray luminosity. The factor $E(z)$, representing the ratio between the Hubble constant at redshift z and its present value, is given, for flat cosmologies, by

$$E^2(z) = \Omega_{0\rm m}(1 + z)^3 + \Omega_\Lambda \,, \tag{9}$$

and allows rescaling all the data to the same redshift (usually $z = 0$).

The SZ self-similar scaling relations have been largely investigated with semi-analytic models (see, e.g., Cavaliere & Menci 2001; Verde et al. 2002; McCarthy et al. 2003) and in numerical hydrodynamic simulations (see, e.g., da Silva et al. 2004; Diaferio et al. 2005; Motl et al. 2005), since deviations from them would indicate that non-gravitational processes, like gas cooling and energy feedback, play an important role in gas-dynamics. It is worth noticing that strong support in favour of a non-negligible role of the non-gravitational processes already comes from the study of self-similar relations in the X-ray band (see, e.g. Cavaliere et al. 1998; Allen & Fabian 1998; Markevitch 1998; Xue & Wu 2000; Borgani et al. 2004; Arnaud et al. 2005; Vikhlinin et al. 2006, and references therein).

We studied the relations in Eqs.(6)-(8) by analysing the same cluster sample of the previous section, but considering each cluster at five different redshifts: $z = 1$, $z = 0.7$, $z = 0.4$, $z = 0.2$, $z = 0$. This corresponds to a time separations ~ 2 Gyr, long enough to allow changes in the cluster dynamical status, and thus to make successive data points from the same cluster roughly independent on each other.

To construct our empirical relations, we used the intrinsic pa-
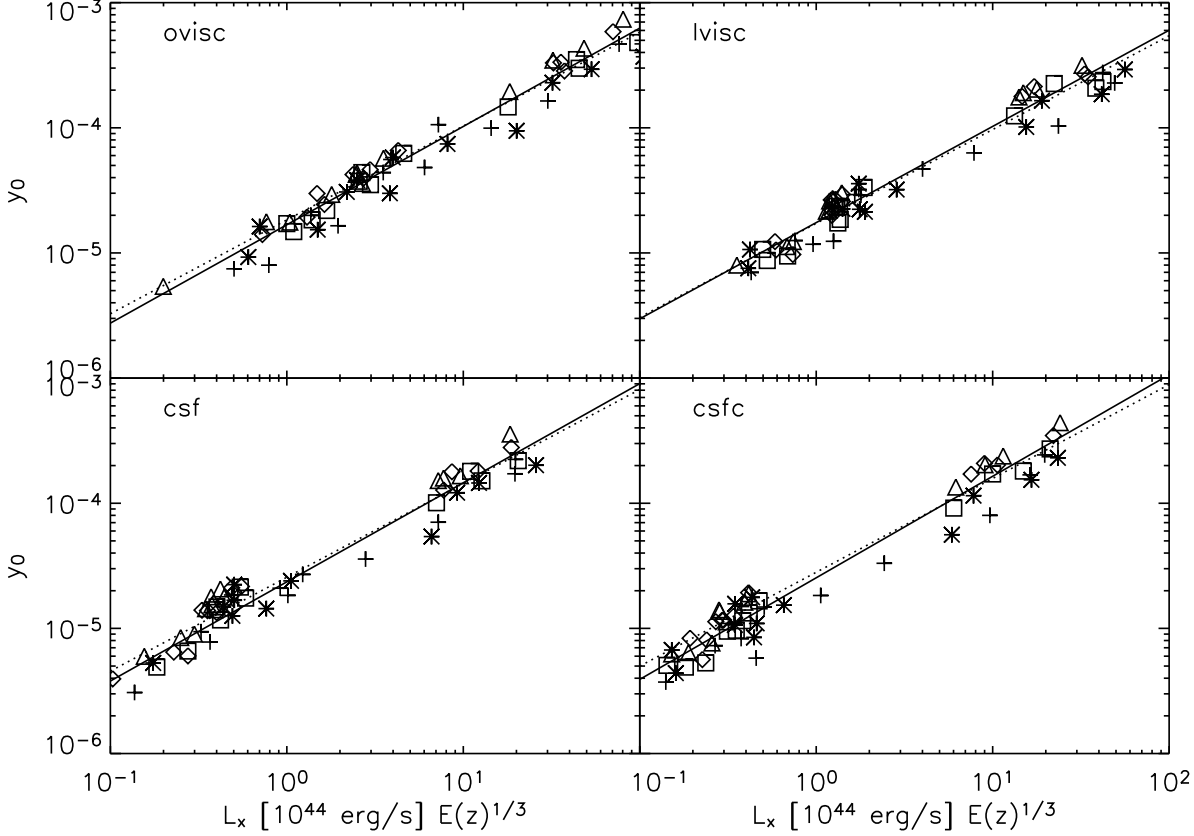
Figure 7. Scaling relation $y_0 - L_X$ for all physics. Solid and dotted lines refer to our best-fit relation and to the best fit obtained by imposing the self-similar slope, respectively. Different symbols refer to clusters at different redshifts, as in Fig. 5.

Table 4. Best-fitting parameters for the different SZ scaling relations ($y_0 - L_X$, $y_0 - T$ and $\Delta S - T$) obtained from our hydrodynamic simulations with different physical modelling of ICM. X-ray luminosity in the [0.1-10 keV] band L_X, mass-weighted temperature T and integrated SZ flux ΔS are given in units of 10^{44} erg/s, keV and mJy/Mpc^2, respectively.

Physics	$y_0 - L_X$ [10^{44} erg/s]
ovisc	$\log(y_0) = (-4.77 \pm 0.01) + (0.78 \pm 0.02) \log(L_X)$
lvisc	$\log(y_0) = (-4.76 \pm 0.01) + (0.77 \pm 0.02) \log(L_X)$
csf	$\log(y_0) = (-4.63 \pm 0.01) + (0.79 \pm 0.02) \log(L_X)$
csfc	$\log(y_0) = (-4.59 \pm 0.01) + (0.81 \pm 0.03) \log(L_X)$

Physics	$y_0 - T$ [keV]
ovisc	$\log(y_0) = (-4.70 \pm 0.03) + (1.54 \pm 0.07) \log(T)$
lvisc	$\log(y_0) = (-4.80 \pm 0.03) + (1.42 \pm 0.06) \log(T)$
csf	$\log(y_0) = (-5.11 \pm 0.03) + (1.71 \pm 0.05) \log(T)$
csfc	$\log(y_0) = (-5.16 \pm 0.01) + (1.75 \pm 0.03) \log(T)$

Physics	ΔS [mJy/Mpc^2] $-T$ [keV]
ovisc	$\log(\Delta S) = (1.68 \pm 0.01) + (2.40 \pm 0.01) \log(T)$
lvisc	$\log(\Delta S) = (1.71 \pm 0.02) + (2.37 \pm 0.02) \log(T)$
csf	$\log(\Delta S) = (1.51 \pm 0.01) + (2.50 \pm 0.01) \log(T)$
csfc	$\log(\Delta S) = (1.53 \pm 0.01) + (2.46 \pm 0.02) \log(T)$

rameters extracted from our SZ maps. The X-ray luminosity in the [0.1-10 keV] band L_X and the integrated SZ flux ΔS were computed within R_{500}. To estimate the temperature we preferred to adopt a mass-weighted estimator: this quantity is in fact related to the energetics involved in the process of structure formation. As shown in earlier papers (Mathiesen & Evrard 2001; Mazzotta et al. 2004; Gardini et al. 2004; Rasia et al. 2005), the alternative of using an emission-weighted temperature - originally proposed to make results from hydrodynamical simulations directly comparable to observational spectroscopic measurements - actually introduces systematic biases when the ICM structure is thermally complex.

First we wish to investigate how the SZ signal is modified by the inclusion of different physical processes. In Fig. 5 we make a one-to-one comparison of the value y_0 obtained for each cluster at a given redshift in the *ovisc* runs versus those obtained in runs including more physics. A similar plot, but for ΔS, is presented in Fig.6. Different symbols refer to different redshifts, as indicated in the figure captions. We find that the values measured in the *csfc* and *csf* runs are systematically lower than for *ovisc*, by a factor ~ 60 per cent for y_0 and of 25 per cent for ΔS. On the other hand, we tested that the plotted data can be fitted with a logarithmic slope which is always compatible with unity, showing that the slope of the relations is robust against changes in the modelled physics.

Let us now turn to the SZ scaling relations. The slope and
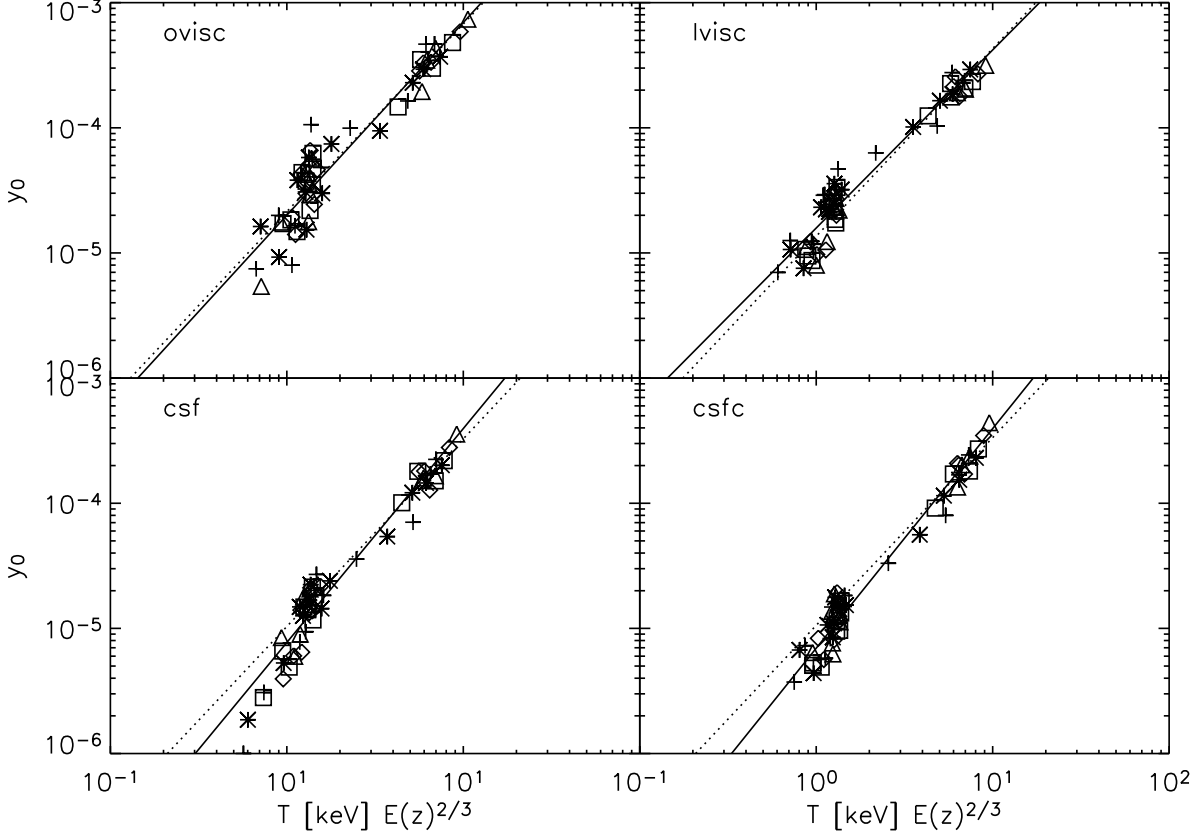
Figure 8. As Fig.7, but for the scaling relation $y_0 - T$.

the normalisation of our best fit relations, with the corresponding errors, have been obtained by applying to each set of parameters (x, y) a "robust" least absolute deviation method. Note that here x and y actually express a log-log relation. First, we fitted the data assuming a linear model $y = A_1 + B_1 x$; we then repeated the linear fitting swapping x and y, and obtained the new parameters (A_2 and B_2). Finally, the slope and intercept (A, B) and the corresponding errors $(\Delta A, \Delta B)$ were calculated as follows:

$$A = (A_1 + A_2)/2 \quad , \quad \Delta A = |A_1 - A_2|/2 \tag{10}$$
$$B = (B_1 + B_2)/2 \quad , \quad \Delta B = |B_1 - B_2|/2. \tag{11}$$

Our best fit relations, reported in Table 4, are also plotted as solid lines in Figs. 7, 8 and 9 for the scaling relations between y_0 and L_X, y_0 and T, and ΔS and T, respectively. For comparison, in each plot the dotted line is the best fit when the self-similar value for the slope is imposed. We first notice that data belonging to different redshifts and corrected by the appropriate factor $E(z)$ define a tight relation: this indicates that the evolution in redshift is in good agreement with predictions of the self-similar model, at least up to $z = 1$. Since our scaling relations were obtained using a sufficiently large number of points, the errors associated to the best fitting slopes and normalizations are relatively small: this increases the statistical significance of our results.

The empirical $y_0 - L_X$ relation for all physics is consistently slightly steeper than the self-similar slope, 0.75; the maximum dif-

ference is ~ 0.05, coming from simulations which include radiative processes. The recovered $y_0 - T$ relation is shallower than the self-similar relation for *lvisc*, while for all other physics it is steeper by $0.1 - 0.2$. Finally, the $\Delta S - T$ relation is very close to the self-similar one (having slope 2.5) for the *csf* runs, but shallower (by 0.05-0.1) for the other ICM models; this conflicts with the work by Nagai (2006), who finds indications (though with no statistical significance) of a slope steeper than the self-similar one.

In general, comparing the values in Table 4 we find that the slope of the relations depends very little on the cluster physics. Similar results were found by Nagai (2006), who reports that introducing radiative cooling lowers the normalization of the $\Delta S - T$ relation, but has no significant impact on the slope. In particular, he finds a normalization lower by 34 per cent, higher than our result. Moreover, we notice that also the *lvisc* clusters exhibit a normalization lower than the *ovisc* ones: part of the pressure is in fact missing, because it was converted into turbulent motions. Note that this process is completely different from the pressure reduction in the runs *csf* and *csfc*, where cooling removes gas from the hot phase in the cluster centre. Of course, it is possible that in nature both processes are acting at the same time. Interestingly, we find that at the centre the signal reduction produced by turbulence and by cooling are comparable in high-mass clusters.
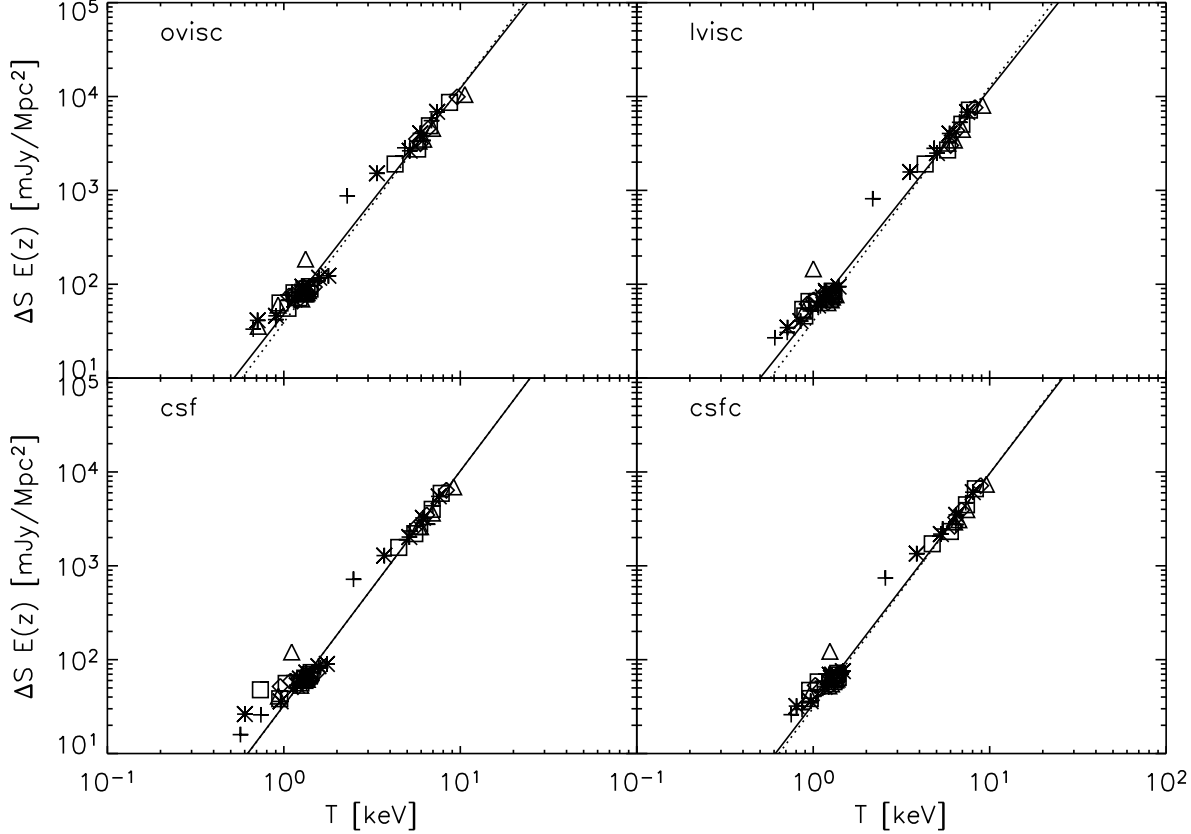
Figure 9. As Fig.7, but for the scaling relation $\Delta S - T$.

6 MOCK OBSERVATIONS

It is now important to verify if the small signatures produced by the different physical processes included in the hydrodynamic simulations discussed above can be detected with a significant signal-to-noise ratio using current SZ instruments. In order to do that, we produced mock observations of our clusters. Among the many dedicated instruments which are planned (see, e.g., Mohr et al. 2002; Lo 2002; Kosowsky 2003; Ruhl et al. 2004), we decided to consider the Arcminute MicroKelvin Imager (AMI; Jones 2002), which is in its commissioning phase in Cambridge (UK)[8] and has already obtained a first detection of a SZ decrement pointing towards the cluster A1914 (Barker et al. 2006). More in detail, AMI is a compact array of 10 small (3.7m) dishes packed together and having a low noise, high-bandwidth back-end system. A complementary array of 8 much larger (13m) dishes will allow the detection and subtraction of unresolved radio sources. Both arrays operate at frequencies of 12-18 GHz. The field of view is 21×21 arcmin.

Obtaining a mock observation with the AMI characteristics requires simulating the response of the interferometric array to some signal on the sky. To do this, we Fourier transformed the image of the simulated cluster, and sampled in the u, v plane according to
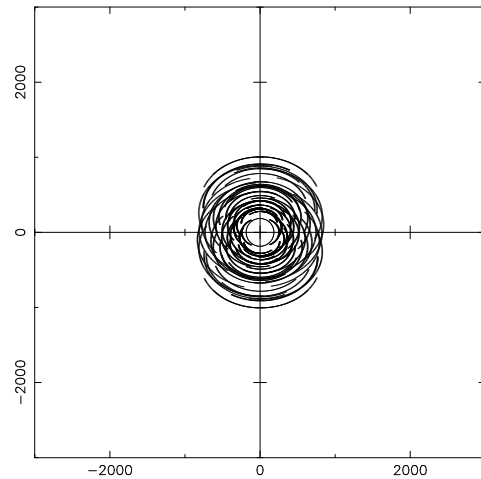
Figure 10. Typical AMI u, v sampling (courtesy of K. Grainge) adopted for our mock observations. It corresponds to a field at dec $50°$ observed at HA=[-4,+4] hours. Axes labels are in units of the wavelength.

the array configuration. The u, v sampling adopted for our observations, and shown in Figure 10, was kindly provided by the AMI collaboration: it corresponds to a field at dec $50°$ and HA [-4, +4] hours.

We then converted our SZ maps from the Comptonization parameter y to a measured flux decrement (given in mJy). We subsequently performed the sampling in the u, v plane and added noise at the appropriate level. Following Kneissl et al. (2001), the noise resulting in the image is $\Delta S_{\rm rms} = 20$ mJy s$^{-1/2}$ over the field of view here considered. In order to reduce noise and spurious structures due to the sampling, we smoothed the map and applied the CLEAN deconvolution algorithm in order to detect the cluster signal. The resulting map, calibrated in flux for the instrumental efficiency, is what we call "observed" cluster.

Notice that in this analysis we do not consider any bias due to CMB fluctuations. The spectrum of primary CMB anisotropies may possess significant power on the largest scales probed by AMI; however, on scales of few arcmin the SZ signal clearly dominates. As we will see, in our case we have good resolution (~ 2 arcmin), and we consider only bright objects, so including the effect of the CMB should not really change our results.

For this observational-like approach we considered the simulated clusters of the HM sample only: in fact, in order to get a signal-to-noise ratio (S/N) good enough to allow robust extraction of radial profiles, the exposure time for small-mass objects would have to be too high. Moreover, we considered the objects at $z = 0.2$: at this redshift our clusters cover a significant part of the field, allowing the instrument to resolve even small structures. The integration time of each simulated observations is $t = 34h$, translating into detections at 10 to 20σ significance. As an example, in Fig.11 we compare one map of the SZ decrement extracted directly from the hydrodynamic simulation to the corresponding one obtained at the end of the AMI observational procedure. The figure refers to the *ovisc* run of cluster *g72a*, which undergoes an important merging event at $z \approx 0.2$. It is evident that in the observed map many details are completely lost and isoflux contours appear more regular. Moreover, the value of SZ decrement at the centre is reduced, as a result of the reduced resolution.

After preparing the individual observations, we extracted the mean profiles as described in the previous sections. The results for clusters simulated including different ICM modelling are shown by the thick lines in Fig. 12. In the same plot, for comparison, we also display as thin lines the mean profiles directly extracted from the hydrodynamic simulations. The ripples in the observed profiles are due to the fact that our simplified removal procedure could not completely cancel spurious structure introduced by the sampling.

As expected, the observational procedure makes it impossible to appreciate differences between SZ profiles produced considering different physical processes. The observed profile is modified by the instrumental beam, so the physics mainly affects the total intensity of the emission. However, this quantity also depends on the cluster mass, and breaking the degeneracy is difficult.

In Table 5 we discuss the robustness of the parameters y_0 and ΔS used in the scaling relations, against the observational process. The central Comptonization parameter y_0 is clearly suppressed by the degraded angular resolution; the amount of suppression depends both on the physics included and on the shape of the specific cluster, ranging from a factor of 1.5 to almost a factor of 2.6 for the *ovisc* run of cluster *g72a*. Conversely, the parameter ΔS is less prone to observational effects; moreover, the amount of this effect is very similar for all clusters and for all physical processes, being always ~ 20 per cent. We can thus say that, with respect to the observational process, the parameter ΔS is much more stable than y_0. As a consequence, the results we found for the $\Delta S - T$ relation should hold even if a properly observed sample of clusters is used.

Table 5. Ratio between the SZ quantities (y_0 and ΔS) extracted directly from simulated clusters and from their mock observations ($y_{0\rm obs}$ and $\Delta S_{\rm obs}$). Columns refer to the different galaxy clusters belonging to HM sample, while rows show the ratios for simulations including different sets of physical processes.

|	g8a	g1a	g72a	g51a
Physics	$y_0/y_{0\rm obs}$			
ovisc	2.24	2.49	2.58	1.97
lvisc	1.73	1.65	1.98	1.45
csf	1.76	1.84	1.93	1.58
csfc	2.16	1.77	2.20	1.75
Physics	$\Delta S/\Delta S_{\rm obs}$			
ovisc	1.19	1.19	1.21	1.18
lvisc	1.21	1.20	1.20	1.22
csf	1.18	1.21	1.17	1.20
csfc	1.18	1.21	1.21	1.21
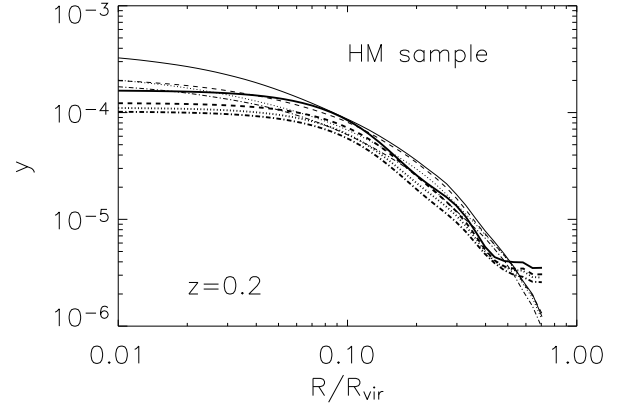
Figure 12. The mean logarithmic SZ profiles obtained from mock observations of simulated galaxy clusters are shown as thick lines. Different lines refer to simulations including different sets of physical processes: line types are as in Fig.3. For comparison, the thin lines refer to the corresponding mean logarithmic SZ profiles directly extracted from the hydrodynamic simulations. Only the HM sample at $z = 0.2$ is considered here.

7 CONCLUSIONS

We used a sample of simulated galaxy clusters with masses ranging from 10^{14} to about $2 \times 10^{15} h^{-1} M_\odot$, re-simulated using different sets of physical processes (radiative cooling, star formation, feedback and thermal conduction) to investigate the dependence of the SZ emission on the ICM physics. Starting from the 3D pressure information, we obtained for each physics fitting relations to the SZ radial profiles. We compared the scaling relations linking cluster central and total SZ flux, and cluster X-ray luminosity and (mass-weighted) temperature, with those predicted by the self-similar model. We then performed mock observations of the most massive systems in our sample, in order to check whether our findings survive the observational procedure. We summarize our main results below.

• The shape of the SZ cluster profile strongly depends on the cluster mass, as a result of the fact that our high mass clusters, at
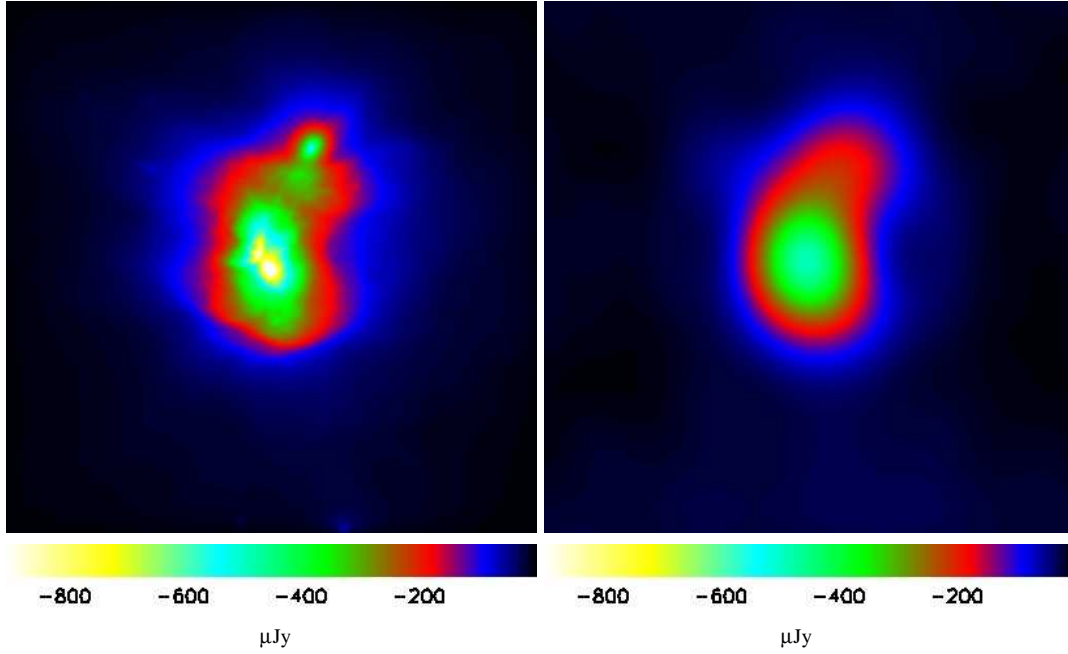
Figure 11. Maps for the SZ decrement for the *ovisc* simulation of cluster *g72a*. The original map extracted from the hydrodynamic simulation, and the same map in the simulated observation ($t = 34h$) which assumes the AMI interferometric response, are shown in the left and right panel, respectively. The side of each map corresponds to 16 arcmin. The colour scale is shown at the bottom of each panel.

variance with the low mass ones, are all isolated and virialized. In particular, while the 3D (logarithmic) pressure profiles of low-mass clusters (LM sample) can be described by a function which is nearly flat for $R \rightarrow 0$ and steepening for $R/R_{\mathrm{vir}} \sim 0.05$, the high-mass clusters (HM sample) exhibit an additional steepening of the profiles at $R/R_{\mathrm{vir}} \sim 0.6$.

• The details of the ICM physics have little impact on the SZ profiles; the largest differences are found near the central regions of low-mass systems.

• The scaling relations between cluster SZ emission and cluster X-ray luminosity and temperature evolve with redshift according to the self-similar model out to $z = 1$; this result is consistent with previous works (da Silva et al. 2004; Motl et al. 2005; Nagai 2006).

• The slopes of the scaling relations for all physics are consistent with the predictions of the self-similar model, even if small discrepancies can still be found: in particular, our empirical relations $y_0 - L_X$ and $y_0 - T$ are generally slightly steeper than the self-similar ones, while the $\Delta S - T$ relation is generally slightly shallower.

• The ICM physics has little effect on the slopes of the scaling relations, in agreement with previous studies (White et al. 2002; Nagai 2006).

• The main effect introduced in the scaling relations by radiative cooling is a lower normalization. If we compare our simulations including cooling with the non-radiative runs with standard viscosity (*ovisc*), we find a suppression of 50 per cent in the central intensity y_0 and of 25 per cent in the integrated flux ΔS. If we compare the cooling plus star-formation runs with the non-radiative ones adopting modified artificial viscosity (*lvisc*), these reductions are of the order of $20 - 30$ per cent. A similar normalization lowering for the $\Delta S - T$ relation was also found by Nagai (2006).

• Our mock observations suggest that arcminute resolution data from the current generation of SZE imaging experiments will not be a sensitive probe of the different physics that is ongoing in the intracluster medium. At arcminute scale angular resolution these effects tend to only have observable consequences on the total cluster flux, which leads to a degeneracy between physics and cluster mass that will be difficult to break

• The integrated flux ΔS is found to be stable against the observational process, and thus should be preferred to y_0, which instead exhibits large variations after performing the mock observations.

REFERENCES

Allen S. W., Fabian A. C., 1998, MNRAS, 297, L57
Arnaud M., Pointecouteau E., Pratt G. W., 2005, A&A, 441, 893

Barker R., et al., 2006, MNRAS, 369, L1

Birkinshaw M., 1999, Phys. Rep., 310, 97

Borgani S., 2006, preprint, astro-ph/0605575

Borgani S., et al., 2004, MNRAS, 348, 1078

Carlstrom J. E., Holder G. P., Reese E. D., 2002, ARA&A, 40, 643

Cavaliere A., Menci N., 2001, MNRAS, 327, 488

Cavaliere A., Menci N., Tozzi P., 1998, ApJ, 501, 493

da Silva A. C., Kay S. T., Liddle A. R., Thomas P. A., 2004, MN-RAS, 348, 1401

Diaferio A., et al., 2005, MNRAS, 356, 1477

Dolag K., Jubelgas M., Springel V., Borgani S., Rasia E., 2004, ApJ, 606, L97

Dolag K., Meneghetti M., Moscardini L., Rasia E., Bonaldi A., 2006, MNRAS, 370, 656

Dolag K., Vazza F., Brunetti G., Tormen G., 2005, MNRAS, 364, 753

Eke V. R., Cole S., Frenk C. S., 1996, MNRAS, 282, 263

Gardini A., Rasia E., Mazzotta P., Tormen G., De Grandi S., Moscardini L., 2004, MNRAS, 351, 505

Jones M. E., 2002, in Chen L.-W., Ma C.-P., Ng K.-W., Pen U.-L., eds, ASP Conf. Ser. 257: AMiBA 2001: High-Z Clusters, Missing Baryons, and CMB Polarization SZ Surveys with the Arcminute MicroKelvin Imager. pp 35–+

Jubelgas M., Springel V., Dolag K., 2004, MNRAS, 351, 423

Kaiser N., 1986, MNRAS, 222, 323

Kneissl R., Jones M. E., Saunders R., Eke V. R., Lasenby A. N., Grainge K., Cotter G., 2001, MNRAS, 328, 783

Kosowsky A., 2003, New Astronomy Review, 47, 939

Lo K. Y., 2002, in Chen L.-W., Ma C.-P., Ng K.-W., Pen U.-L., eds, ASP Conf. Ser. 257: AMiBA 2001: High-Z Clusters, Missing Baryons, and CMB Polarization The Current State of Astronomy in Taiwan and AMiBA. pp 3–+

Markevitch M., 1998, ApJ, 504, 27

Mathiesen B. F., Evrard A. E., 2001, ApJ, 546, 100

Mazzotta P., Rasia E., Moscardini L., Tormen G., 2004, MNRAS, 354, 10

McCarthy I. G., Babul A., Holder G. P., Balogh M. L., 2003, ApJ, 591, 515

Mohr J. J., Carlstrom J. E., The Sza Collaboration 2002, in Chen L.-W., Ma C.-P., Ng K.-W., Pen U.-L., eds, ASP Conf. Ser. 257: AMiBA 2001: High-Z Clusters, Missing Baryons, and CMB Polarization The SZ-Array: Configuration and Science Prospects. pp 43–+

Morris J. P., Monaghan J. J., 1997, J. Comp. Phys., 136, 41

Motl P. M., Hallman E. J., Burns J. O., Norman M. L., 2005, ApJ, 623, L63

Nagai D., 2006, ApJ, 650, 538

Navarro J. F., Frenk C. S., White S. D. M., 1995, MNRAS, 275, 720

Rasia E., Mazzotta P., Borgani S., Moscardini L., Dolag K., Tormen G., Diaferio A., Murante G., 2005, ApJ, 618, L1

Rasia E., Tormen G., Moscardini L., 2004, MNRAS, 351, 237

Rephaeli Y., Sadeh S., Shimon M., 2005, in Melchiorri F., Rephaeli Y., eds, Background Microwave Radiation and Intracluster Cosmology The Sunyaev-Zeldovich effect. pp 57–+

Roncarelli M., Moscardini L., Tozzi P., Borgani S., Cheng L. M., Diaferio A., Dolag K., Murante G., 2006, MNRAS, 368, 74

Rosati P., Borgani S., Norman C., 2002, ARA&A, 40, 539

Ruhl J., et al., 2004, in Zmuidzinas J., Holland W. S., Withington S., eds, Astronomical Structures and Mechanisms Technology. Edited by Antebi, Joseph; Lemke, Dietrich. Proceedings of the SPIE, Volume 5498, pp. 11-29 (2004). The South Pole Telescope. pp 11–29

Springel V., 2005, MNRAS, 364, 1105

Springel V., Hernquist L., 2002, MNRAS, 333, 649

Springel V., Hernquist L., 2003, MNRAS, 339, 289

Springel V., Yoshida N., White S. D. M., 2001, New Astronomy, 6, 79

Sunyaev R. A., Zeldovich Y. B., 1972, Comments on Astrophysics and Space Physics, 4, 173

Tormen G., Bouchet F. R., White S. D. M., 1997, MNRAS, 286, 865

Verde L., Haiman Z., Spergel D. N., 2002, ApJ, 581, 5

Vikhlinin A., Kravtsov A., Forman W., Jones C., Markevitch M., Murray S. S., Van Speybroeck L., 2006, ApJ, 640, 691

Voit G. M., 2005, Reviews of Modern Physics, 77, 207

White M., Hernquist L., Springel V., 2002, ApJ, 579, 16

White S. D. M., 1996, in Schaeffer R., Silk J., Spiro M., Zinn-Justin J., eds, Cosmology and Large Scale Structure Formation and Evolution of Galaxies. pp 349–+

Xue Y.-J., Wu X.-P., 2000, ApJ, 538, 65

Yoshida N., Sheth R. K., Diaferio A., 2001, MNRAS, 328, 669